

# Reconciling Translational Invariance and Hierarchy

Olai B. Mykland<sup>1,2</sup> and Zhao Zhang<sup>1</sup>

<sup>1</sup>Department of Physics, University of Oslo, P.O. Box 1048 Blindern, N-0316 Oslo, Norway

<sup>2</sup>Department of Physics, Norwegian University of Science and Technology, NO-7491 Trondheim, Norway

Tensor networks are not only numerical tools for describing ground states of quantum many-body systems, but also conceptual aids for understanding their entanglement structures. The proper way to understand tensor networks themselves is through explicit examples of solvable ground states that they represent exactly. In fact, this has historically been how tensor networks for gapped ground states, such as the matrix product state (MPS) and the projected entangled paired state (PEPS), emerged as an elegant analytical framework from numerical techniques like the density matrix renormalization group. However, for gapless ground states, generically described by the multiscale entanglement renormalization ansatz (MERA), a corresponding exactly solvable model has so far been missing. This is because the hierarchical structure of MERA intrinsically breaks the translational invariance. We identify a condition for MERA to be compatible with translational invariance by examining equivalent networks of rank-3 tensors. The condition is satisfied by the previously constructed hierarchical tensor network for the Motzkin and Fredkin chains, which can be considered a non-unitary generalization to the MERA. The hierarchical TN description is complemented by a translationally invariant MPS alternative, which is used to derive the power-law decay of the correlation function and critical exponents of a  $q$ -deformation phase transition.

## 1 Introduction

Efficient numerical simulations of quantum many-body systems are dependent on accurate understandings of the entanglement patterns of their ground states (GSs) and low energy excited states. As wavefunctions, they are specified by a multivariate function, with configurations of the physical degrees of freedom as inputs and the probability amplitude as the output. For a system consisting of  $N$  degrees of freedom, this is a rank- $N$  tensor. In order for it to be useful for information storage or manipulation, it has to be decomposed into lower rank tensors. In condensed matter physics, systems of interest usually have their degrees of freedom living on a regular lattice. The tensor decomposition should therefore respect the discrete symmetries of the physical lattice. The simplest decomposition into a 1D translationally invariant contraction of rank-3 tensors is the tensor train. The rank three is special in that further decompositions would only increase the number of tensors without lowering their ranks. This is indeed what the density matrix renormalization group (DMRG) [1] algorithm produces, except that the definitions of the tensors are different from site to site. To fully exploit the translation symmetry, one can start with a

---

Zhao Zhang: [zhao.zhang@fys.uio.no](mailto:zhao.zhang@fys.uio.no)

trial state described by a matrix product of identical rank-3 tensors, to be determined from variational algorithms such as infinite time-evolving block decimation (iTEBD) [2].

The leap from DMRG as a sequential optimization technique to matrix product state (MPS) [3, 4] as a schematic theory for describing generic gapped GSs is largely facilitated by the realization that MPS provides an exact description of the GSs of the AKLT chain [5, 6] and Majumdar-Ghosh chain [7, 8]. 2D versions of the valance bond solid states [9] have also lead to the generalization of MPS to projected entangled paired states (PEPSs) [8, 10]. The success story continued to multicomponent generalizations to simplex solid states [11], which inspired the proposal of projected entangled simplex states [12].

Contrary to the development of tensor networks (TNs) for gapped GSs, the TN description for gapless GSs called the multiscale entanglement renormalization ansatz (MERA) was proposed first without the inspiration from any specific exactly solvable GS [13]. Although plenty of GSs well approximated by the MERA were found later, especially for free fermions [14, 15], a GS described exactly by the MERA is to date missing. Unlike MPSs which have short-range entanglement that can be generated by a finite depth quantum circuit, at quantum critical points, GSs violate the area law of entanglement entropy (EE) [16] logarithmically, which means that the TN should have a hierarchical structure and extends to an extra dimension beyond the physical lattice.

The simplest hierarchical TN is the tree tensor network, which is the outcome of the tensor renormalization group (TRG) procedure [17, 18] on a 2D TN with open boundaries. However, this approach leaves short-range correlations intact in the renormalization group (RG) flow. To correctly describe critical fixed points, Evenly and Vidal introduced the tensor network renormalization (TNR), which removes short-range correlations by a unitary disentangler between nearest neighbors before each iteration of the RG transformation [19]. The resulting TN structure of the MERA is therefore composed of rank-3 isometries and rank-4 disentanglers, but a unit cell containing one of each is a rank-5 tensor. So the key difference between the MERA and tree tensor network, which consists purely of rank-3 tensors, is that the former is able to capture just as well the entanglement within each level of the coarse-grained degrees of freedom, hence entanglement at all different length scales.

In order to construct an exactly solvable GS with long-range entanglement, a frustration free Hamiltonian was proposed by Bravyi et al. [20]. The model describes a spin-1 system later called the Motzkin chain, and in many ways it can be considered a more entangled version of the AKLT chain. A TN representation of the GS is constructed as the first exact TN for critical ground states [21], which also has building blocks of rank three and four. The authors marked its resemblance with the MERA, but emphasized the absence of either isometry or unitarity. We notice that both TNs have their unit cells being rank-5 tensors, and should be able to transform into one another through a series of singular value decompositions (SVDs) and contractions of internal legs. Alternatively, they amount to different tensor decompositions of a rank-5 tensor into tensors of rank three and four. There is thus a trade-off between informativeness and uniformness for TN representations of the same state with higher or lower ranked tensors. While every TN can be decomposed into products of rank-3 tensors alone, choosing a higher ranked tensor can reduce the arbitrariness of TN definitions to merely gauge degrees of freedom. For 1D MERA, we identify five as the smallest rank for different TNs describing the same state to share the same geometrical structure.

Different rank-3 tensor decompositions of the same rank-5 tensor are constrained by a pentagon identity, as there are multiple series of SVDs that bring one decomposition to another. Similarly, a layer of the MERA can be shifted horizontally by one lattice site through a sequence of SVDs. Requiring the tensors after the transformations to be the same

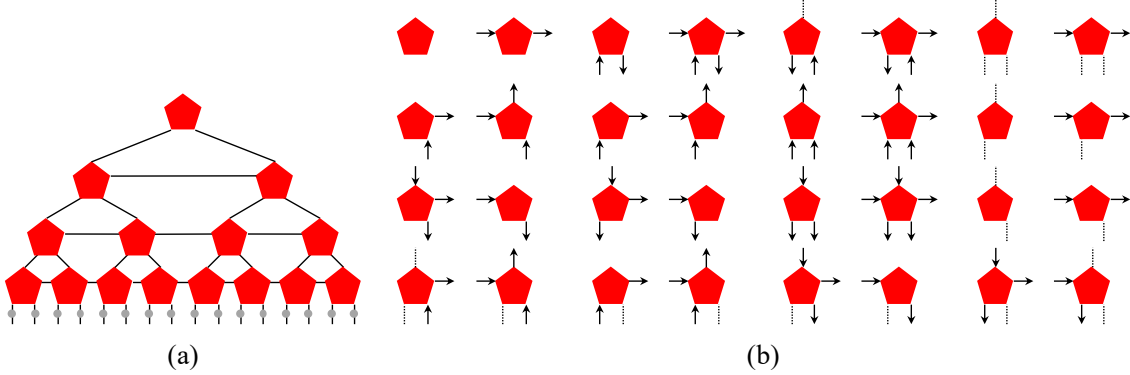


Figure 1: (a) Pentagonal TN for the GS of a Motzkin chain of length 16. (b) The 32 non-vanishing entries of the rank-5 tensor in the bulk. The tensors on the boundary of the network has rank two or four, depending on its location, and is only non-vanishing for the corresponding compatible configurations.

as before, we obtain a local condition for the MERA to be translationally invariant. This condition is satisfied by the Motzkin TN, which explains the existence of its translationally invariant parent Hamiltonian.

The unification between translational invariance and hierarchy is achieved in this article also by an MPS description of the Motzkin and Fredkin GS. An MPS description of the Fredkin GS with growing bond dimension was first proposed in Ref. [22], as an approximation method when the bond dimension is truncated. Here, we restore the translational invariance by adopting a uniform tensor definition along the chain, and use it to construct a transfer matrix (TM) that allows the analytical derivation of the power-law decay of correlation and the value of the critical exponent  $\eta$ . From the scaling dimension of the spin operator deduced from the TM calculation, an RG analysis is applied to the  $q$ -deformed GSs studied in the colored version of the Motzkin and Fredkin models with entanglement phase transition [23, 24, 25, 26, 27, 28, 29], which enables the computation of the critical exponent  $\nu$ .

The rest of the article is structured as follows. Sec. 2 reviews the TN representation of the Motzkin GS starting from rank-5 tensors, and transform it into the shape of a MERA network. Sec. 3 examines the condition for MERA to be translationally invariant, satisfied by the TN in the previous section. Sec. 4 constructs a TM from the MPS representation of the GS with a bond dimension that scales with the system size, to be used for finding the spatial decay behavior of the correlation. Sec. 5 shows the power-law decay of the order parameter at the critical point, which reflects the correlation with the boundary spins. Sec. 6 uses the scaling dimension of the spin operator deduced from the TM result to find the critical exponent  $\nu$  from RG analysis when the GS is  $q$ -deformed away from the critical point. The analytical critical exponents  $\eta$  and  $\nu$  are both confirmed by numerical results from MPS calculations. Finally, Sec. 7 concludes the article by pointing out a few future directions to explore.

## 2 Pentagonal TN for the Motzkin GS

A TN representation of the GS of a Motzkin chain of length  $L = 8$  using only rank-5 tensors is presented in Fig. 1 (a), with the configurations listed in Fig. 1 (b) of value 1 and all the rest of value 0. A pentagonal tensor corresponds to the contraction of a triangular tensor with two squares below it according to the definitions in Ref. [21], and are listed

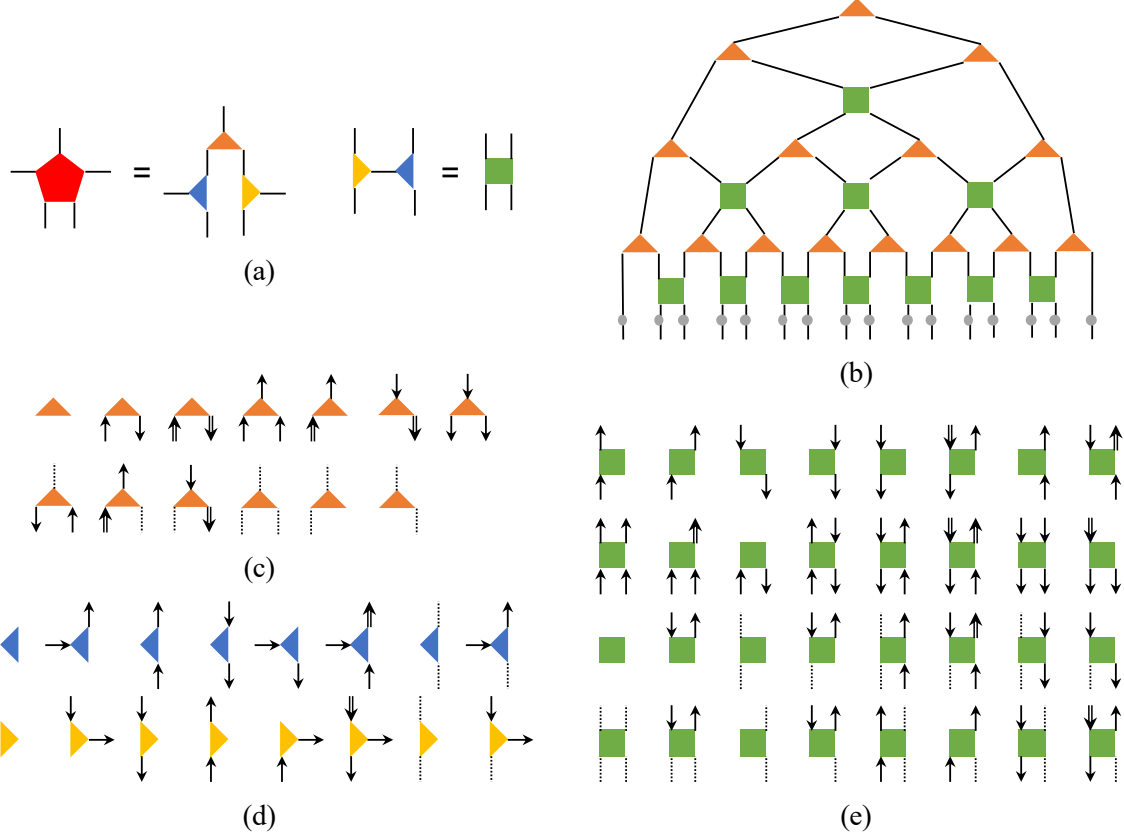


Figure 2: (a) Decomposition of a rank-5 tensor into the product of three rank-3 tensors, and recombination of two of the rank-3 tensors into a rank-4 tensor. (b) Equivalent representation of the pentagonal TN in Fig. 1 (a) using rank-3 and 4 tensors. (c)-(e) List of tensor configurations for the four types of tensors with value 1. Tensor entries for the rest of the configurations all have value 0.

in Fig. 11 and 12 of its Appendix D and E. Each horizontal leg has bond dimension two, while each vertical leg is of dimension 4. So there are 32 out of the  $2^2 \cdot 4^3 = 256$  possible combinations that give non-vanishing elements of the tensor, obviously a very sparse one. Each of the external legs on the bottom layer is attached to a projection operator that projects out the unphysical degrees of freedom denoted by the dotted line (and the empty leg for the spin- $\frac{1}{2}$  Fredkin model described by the same TN).

The three legs on the left and bottom of a pentagon can be labeled as the input indices, and the top and right ones the output. Ignoring the dotted lines for the moment, an arrow flowing inward (resp. outward) is considered +1 (resp. -1) for the input legs, and the opposite for the output, while an empty leg is treated as 0. Then each pentagonal tensor corresponds to a binary addition, with the top leg encoding the carry digit. This represents a coarse-graining mapping from the spins in the level below to the level above. Two up- or down-spins are of course mapped to up and down respectively, and one up one down is mapped to spin zero. But what one up one zero or one down one zero maps to is dependent on the leftover spin from the string of tensors on the same level to the left. The role of the dotted line is to keep track of reverse ordered up-down spin neighboring pairs. This is important for the GS to be a superposition of only spin configurations that correspond to Motzkin paths, namely to always have at least as many up spins as down spins to the left at any point along the chain. Therefore, two dotted lines merge into one, and a dotted line disappears in the level above if the horizontal legs of the tensor has nonzero values.

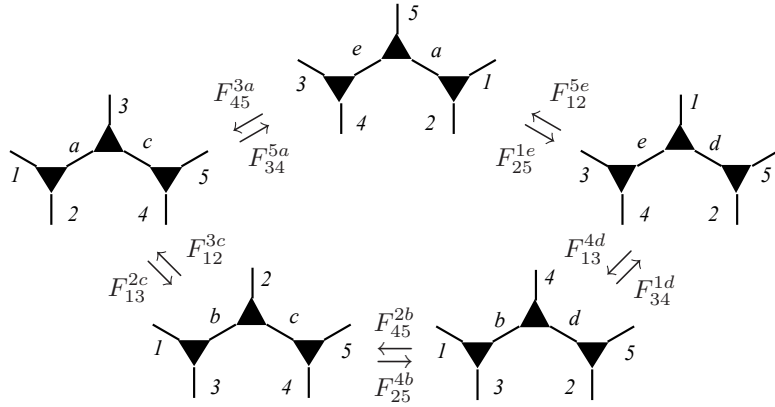


Figure 3: Pentagonal identity for the  $F$  symbols of transformations among different decompositions of the same 5-leg tensor.

As shown on the left panel of Fig. 2 (a), the pentagons can be decomposed into the product of three rank-3 tensors shown in Fig. 2 (c) and (d), two of which (Fig. 2 (d)) can be combined between neighboring tensors following the right panel of Fig. 2 (a) to form the rank-4 tensor in Fig. 2 (e). As already remarked in Ref. [21], the difference between the TN in Fig. 2 (b) and the MERA is that the 4-leg tensor is not unitary (although the 3-leg tensor in Fig. 2 (c) can be made isometric by letting the upper legs of the tensors in Fig. 2 (d) absorb a constant factor.) Instead of separating disentangling and coarse-graining into two separate tensors, the coarse-graining is done at both stages. But this opens the door to translational invariance. In the MERA structure, disentangling happens only between even-odd neighboring pairs. This means that the first level of the TN breaks translational invariance into translations by two lattice spacings, which is further broken at the next level to translations by 4 lattice spacings, and so on so forth. So the hierarchical structure of the TN completely breaks the translational invariance. This is the reason that so far, there has not been an exactly solvable Hamiltonian that has a GS described exactly by the MERA. Therefore, at the possible sacrifice of efficiency in the computation of correlation functions, the pentagonal TN in Fig. 1 (a) is proposed as a generalization to the MERA that is in principle compatible with translational invariance.

### 3 Translationally invariant MERA

In order to obtain a criterion for the hierarchical structure of the MERA to be also translationally invariant, we study the transformations among different decompositions of generic TNs into products of rank-3 tensors. As already argued in the introduction, they are the fundamental building blocks of a TN, in the sense that they cannot be further decomposed into tensors with lower ranks. A decomposition of the TN can be viewed as a choice of basis for the tensor it represents. A three-leg tensor can therefore be viewed as a fusion process, and the basis transformations denoted by the so-called  $F$  symbols are subject to consistency equations called the pentagon identity. As illustrated in Fig. 3, there are two different sequences of transformations that relate the decomposition on the left to that on the right, demanding

$$[F_{25}^{1e}]_a [F_{34}^{5a}]_c^e = [F_{34}^{1d}]_b^e [F_{25}^{4b}]_c^d [F_{13}^{2c}]_a^b. \quad (1)$$

According to the coherence theorem by Mac Lane [30], this identity alone guarantees that all different decompositions related by more  $F$ -symbols are mutually compatible.

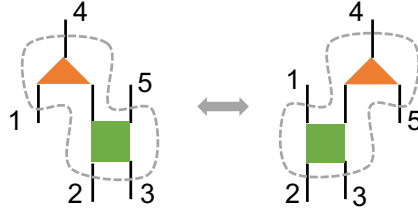


Figure 4: Local  $F$  moves that shifts a slice of a hierarchical TN structure by one lattice spacing.

For a TN with the same geometry as the MERA to be translationally invariant, it needs to return to itself after shifting by one lattice spacing. The global shift can be implemented by the local move shown in Fig. 4. Translational invariance means that the rank-3 and 4 tensors after the transformation is identical to those before. It is straightforward though tedious to check that this relation is indeed satisfied by the definitions in Fig. 2, which explains that the Motzkin GS as a GS for a translationally invariant Hamiltonian is exactly described by a hierarchical TN. Enforcing this constraint on numerical simulations using the MERA might also improve the accuracy of describing translationally invariant states.

## 4 Transfer matrix from the MPS

The generalized MERA network, without unitarity and isometry of the consisting tensors, do not facilitate efficient evaluation of the expectation values and correlation functions of local operators in the Fredkin and Motzkin GS as the original MERA does [31]. Instead, we found a way to do that using the MPS representation. In theory, MPSs can only describe 1D gapped systems, even though it is common practice for numerical experts to use MPS with large bond dimensions for simulating 1D gapless states. Since the Motzkin and Fredkin GSs are the first examples of exact MPSs with bond dimensions that grows with the system size, we can use the exact transfer matrices constructed from the MPS representations to analytically study the correlation and critical behavior near the phase transition of the  $q$ -deformation reviewed in Appendix D.

The expectation value of spins and their correlations have been obtained before using asymptotics of combinatorial results [32, 33] and Gaussian free field description in the scaling limit [34]. Here we present a much more transparent derivation using the TM method, from which the critical exponents  $\eta, \nu$  defined by

$$\langle O_1 O_r \rangle \propto \begin{cases} r^{2-d-\eta}, & \text{for } q = 1, \\ e^{-r/\xi}, & \text{for } q < 1, \text{ with } \xi \propto (\log q)^{-\nu} \end{cases} \quad (2)$$

can be extracted. Due to the opposite boundary conditions on different ends of the chain, the two-point correlation in the ordered phase  $q > 1$  is not a constant. This will be discussed in detail in Sec. 6. The Hamiltonians of the Motzkin and Fredkin chains (reviewed in Appendix D) explicitly break the symmetry between up and down spins at the boundary of a finite sized system. Hence the correlation between the spin at distance  $r$  with the constant valued boundary spin in the GS can be probed from the skin-depth of the boundary effect, instead of the two-point correlation function as defined in Eq. (2). Thus, we can find the critical exponents by computing the one-point function  $\langle S_r^z \rangle$ .

The exact MPS representation of the Fredkin GS was given in Ref. [22] at the critical value  $q = 1$  of the deformation parameter  $q$ . In the MPS, the bond dimension of internal legs is  $L + 1$  for a chain of length  $2L$ , which follows from the maximum height of a

Dyck walk of  $2L$  steps. The  $L$ -dependent bond dimension enable the MPS to capture the unusual scaling of the entanglement entropy in the state, which scales as  $\log L$ . We now construct the MPS representation of the Motzkin GS, which is done by simply considering the Motzkin walks instead of the Dyck walks. We also generalize both MPSs to represent the GSs at all values of  $q$ . This is achieved by weighing tensor elements by factors of  $q$  that depend on the height  $h$  (or equivalently the area  $A(w)$ ) of the walk  $w$  in the GS superposition Eq. (45). The GS is then represented as

$$\begin{aligned} |\text{GS}\rangle &= \frac{1}{\sqrt{C}} \sum_{\{s_j\}} A_{0h_2}^{(s_1)} A_{h_2h_3}^{(s_2)} \cdots A_{h_{2L}0}^{(s_{2L})} |\{s_j\}\rangle, \\ &= \frac{1}{\sqrt{C}} \bullet \xrightarrow{A^{(s_1)}} \xrightarrow{A^{(s_2)}} \cdots \xrightarrow{A^{(s_{2L})}} \bullet \end{aligned} \quad (3)$$

In the first line, Einstein's summation convention applies to the internal indices  $h_j$ . The physical spin indices are denoted  $s_j$  and its values corresponds to the eigenstates of  $S_j^z$  for site  $j$ . Naturally, for the Fredkin MPS it takes on two values  $s_j = [-1, 1]$ , while for the Motzkin MPS it takes on three values  $s_j = [-1, 0, 1]$ . In the second line, we have written the MPS diagrammatically, where each open leg corresponds to a spin  $s_j$  and the black dots denote boundary tensors  $\delta_{h_i0}$ , fixing the indices  $h_1$  and  $h_{2L+1}$  to 0.  $C = \langle \text{GS} | \text{GS} \rangle$  is the normalization constant. The matrices  $A^{(s_j)}$  are defined as

$$A_{h_j h_{j+1}}^{(s_j)} = q^{h_j \pm \frac{s_j}{2}} \delta_{h_j, h_{j+1} \pm s_j}. \quad (4)$$

We have  $0 \leq h_j \leq L$ , meaning that the bond dimension of the MPS is  $L + 1$ . The MPS is implemented in ITensor [35] for both the Fredkin and Motzkin GSs and used to compute expectation values. The results will be presented in the next two sections.

The TM  $\mathcal{T}$  is constructed by contracting the physical external legs of matrices  $A^{(s_j)}$  and their conjugate  $\bar{A}^{(s_j)} = A^{(s_j)}$

$$\begin{aligned} \mathcal{T}_{h_j, h'_j; h_{j+1}, h'_{j+1}} &= \sum_{s_j = \pm 1, (0)} A_{h_j, h_{j+1}}^{(s_j)} \bar{A}_{h'_j, h'_{j+1}}^{(s_j)} \\ &= q^{h_j + h'_j} \left[ q \delta_{h_j, h_{j+1} + 1} \delta_{h'_j, h'_{j+1} + 1} + q^{-1} \delta_{h_j + 1, h_{j+1}} \delta_{h'_j + 1, h'_{j+1}} \left( + \delta_{h_j, h_{j+1}} \delta_{h'_j, h'_{j+1}} \right) \right]. \end{aligned} \quad (5)$$

The first term corresponds to spin up, the second term to spin down and the third term to spin-0 (only present in the Motzkin case), with  $0 \leq h_j, h'_j \leq L$  for all  $j$ . From now on, we suppress the four indices of the TM and write  $\mathcal{T}$ . We can also write Eq. (5) diagrammatically as seen in Fig. (5) (a) for the Fredkin case.

The indices  $h_j$  and  $h'_j$  can in general take on any value between 0 and  $L$ , but the non-vanishing entries of the TM satisfy  $h_j - h_{j+1} = h'_j - h'_{j+1} = \pm 1$ , or additionally 0 for Motzkin. This means that the TM is block diagonal. Furthermore, each block is a symmetric matrix, due to the parity between the physical spin configurations being contracted. The TM thus corresponds to the adjacency matrix for a disjoint union of path graphs. The adjacency matrix and corresponding path graph is seen for the  $L = 2$  system for the Fredkin chain in Fig. (5) (b). Note that the two numbers marking the rows (resp. columns) denote the values of the  $h_j h'_j$  (resp.  $h_{j+1} h'_{j+1}$ ) indices. In the Motzkin TM one also has nonzero entries on the diagonal corresponding to flat moves in the Motzkin walks and thus loops in the graph that connect nodes to themselves. In general the  $\mathcal{T}$  is

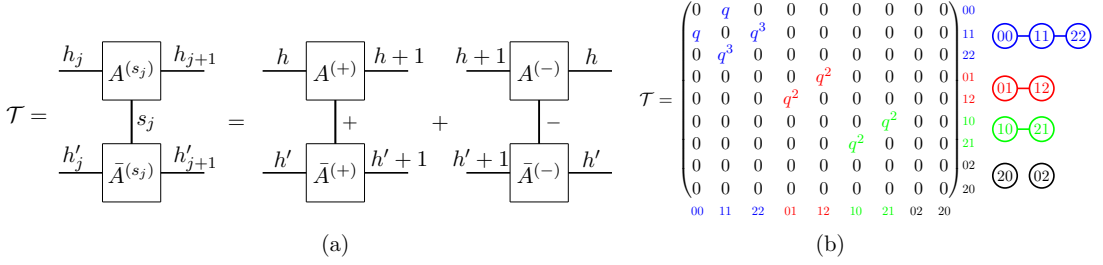


Figure 5: (a) Diagrammatic depiction of the Fredkin TM (left) and its nonzero elements (right), where  $0 \leq h, h' \leq L - 1$ . (b) The block diagonal Fredkin TM for  $L = 2$ , and the corresponding disjoint path graphs. The two numbers marking the rows (resp. columns) denote the values of the  $h_jh'_j$  (resp.  $h_{j+1}h'_{j+1}$ ) indices and the nodes in the graph are labeled by the values of the indices of the TM.

written as

$$\mathcal{T} = \bigoplus_{b=1}^{2L+1} T_b = \begin{pmatrix} T_1 & 0 & \cdots & 0 \\ 0 & T_2 & \cdots & 0 \\ \vdots & \vdots & \ddots & \vdots \\ 0 & 0 & \cdots & T_{2L+1} \end{pmatrix}, \quad (6)$$

where  $\oplus$  is the direct sum. Each block  $b$  of dimension  $d_b$  corresponds to one of the path graphs and the corresponding matrix  $T_b$  is given as the adjacency matrix to that graph, with  $q$ -dependent weights (see Fig. (5) for the  $L = 2$  case). The critical exponents will be computed by evaluating expectation values. They can be computed from the TM as

$$\begin{aligned} \langle O_r \rangle &= \frac{1}{C} \langle 00 | \mathcal{T}^{r-1} \mathcal{T}_O \mathcal{T}^{2L-r} | 00 \rangle, \\ &= \frac{1}{C} \langle 00 | \mathcal{T}^{r-1} \mathcal{T}_O \mathcal{T}^{2L-r} | 00 \rangle, \end{aligned} \quad (7)$$

where  $\mathcal{T}_O$  is given as

$$(\mathcal{T}_O)_{h_j, h'_j; h_{j+1}, h'_{j+1}} = \sum_{s, s'=\pm} A_{h_j, h_{j+1}}^{(s)} O_{ss'} \bar{A}_{h'_j, h'_{j+1}}^{(s')}. \quad (8)$$

The boundary conditions fixing the start and endpoints of the chain to zero height, are enforced by multiplication with the unit vector  $|00\rangle \doteq (1 \ 0 \ \dots \ 0)$ , where we use the same basis as the TM is written in Fig. (5) (b).

Inserting the spectral decomposition of  $\mathcal{T}$ , found by decomposing each individual block  $T_b$ , gives

$$\langle O_r \rangle = \frac{1}{C} \sum_{b=1}^{2L+1} \sum_{k_1, k_2=1}^{d_b} \lambda_{k_1}^{r-1} \lambda_{k_2}^{2L-r} \langle 00 | k_1^b \rangle \langle k_1^b | \mathcal{T}_O | k_2^b \rangle \langle k_2^b | 00 \rangle. \quad (9)$$

Note that the entries of the eigenvectors  $|k_i^b\rangle$  lying outside block  $b$  are 0. This means that  $\langle 00 | k^b \rangle = 0$  if  $b$  is not the block in the upper left corner marked by two equal numbers, see Fig. (5) (b). This matrix block has the largest dimension of any block, with dimension  $d_{\max} = L + 1$ . We denote this matrix by  $T_{\max}^F$  and  $T_{\max}^M$  for the Fredkin and Motzkin case

respectively, and they have the following tridiagonal forms

$$(T_{\max}^F)_{jl} = \begin{cases} q^{j+l-2}, & |j-l|=1, \\ 0, & \text{otherwise,} \end{cases} \quad (T_{\max}^M)_{jl} = \begin{cases} q^{j+l-2}, & |j-l| \leq 1, \\ 0, & \text{otherwise,} \end{cases} \quad (10)$$

with  $j, l \in [1, \dots, L+1]$ . Thus, Eq. (9) can be rewritten only in terms of the eigendecomposition of  $T_{\max}$ , which reads

$$\begin{aligned} \langle O_r \rangle &= \frac{1}{C} \sum_{k_1, k_2=1}^{d_{\max}} \lambda_{k_1}^{r-1} \lambda_{k_2}^{2L-r} \langle 00|k_1\rangle \langle k_1|T_O|k_2\rangle \langle k_2|00\rangle, \\ &= \frac{1}{C} \sum_{k_1, k_2=1}^{d_{\max}} \lambda_{k_1}^{r-1} \lambda_{k_2}^{2L-r} c_{k_1} T_O^{k_1 k_2} c_{k_2}, \end{aligned} \quad (11)$$

where we have denoted the eigenvectors of  $T_{\max}$  as  $|k_i\rangle$ . We have also defined  $c_{k_i} = \langle 00|k_i\rangle = \langle k_i|00\rangle$  and  $T_O^{k_1 k_2}$  as

$$T_O^{k_1 k_2} = \langle k_1|T_O|k_2\rangle = \sum_{j, l=1}^{d_{\max}} {}_j\langle k_1|({T_O})_{jl}|k_1\rangle_l. \quad (12)$$

Since the components of  $|k_i\rangle$  vanish outside subspace of the maximum block, we can restrict the sum to indices  $j, l$  within the block  $T_{\max}$ . As an immediate consequence of this, we get  $\langle S_r^x \rangle = \langle S_r^y \rangle = 0$  for all  $r$ . This is seen by inserting the Pauli matrices  $\sigma_x$  and  $\sigma_y$  for  $O$  in Eq. (8). Since these Pauli matrices act as ‘bit flips’, we find that all entries located by two indices denoted by two equal numbers, that is the indices within  $T_{\max}$ , are zero. Thus, for the ground state of the deformed Fredkin spin chain we have  $\langle S_r^x \rangle = \langle S_r^y \rangle = 0$  for all  $r$  and for all values of  $q$ . This matches previous results for the  $q=1$  GS of the Motzkin and Fredkin chain [32, 36].

## 5 Critical correlation from the transfer matrix method

For gapped GSs, the long distance behavior of Eq. (11) is dominated by the largest two eigenvalues of the transfer matrix. When the system is gapless, as is the case of the models in question at the critical point  $q=1$ , the spectrum of the TM is continuous in the thermodynamic limit. Luckily, for  $q=1$ , the matrices  $T_{\max}^{F/M}$  in Eq. (10) becomes Toeplitz, and their eigensystems have closed-form expressions that allow us to convert the discrete sum in Eq. (11) to an integral.

A  $d_{\max}$ -dimensional tridiagonal Toeplitz matrix with 0 (Fredkin case) or 1 (Motzkin case) on the diagonal and 1 on its super- and subdiagonal has eigenvalues  $\lambda_k$  and eigenvectors  $|k\rangle$  for  $1 \leq k \leq d_{\max}$  given by

$$\lambda_k = \begin{cases} 2 \cos\left(\frac{k\pi}{d_{\max}+1}\right), & \text{Fredkin,} \\ 1 + 2 \cos\left(\frac{k\pi}{d_{\max}+1}\right), & \text{Motzkin,} \end{cases} \quad |k\rangle = \sqrt{\frac{2}{d_{\max}}} \begin{pmatrix} \sin\left(\frac{k\pi}{d_{\max}+1}\right) \\ \sin\left(\frac{2k\pi}{d_{\max}+1}\right) \\ \vdots \\ \sin\left(\frac{d_{\max}k\pi}{d_{\max}+1}\right) \end{pmatrix}. \quad (13)$$

Clearly,  $T_{\max}^{F/M}$  is gapless for  $q=1$  in the large  $L$  limit, as  $d_{\max} = L+1$ . As discussed in Sec. 4, to estimate the critical exponent  $\eta$  normally associated with the connected

correlation function in the critical phase, we will compute the one-point function  $\langle S_r^z \rangle$ . To that end, we insert the matrix representation of  $S^z$ , the spin- $\frac{1}{2}$  (resp. spin-1) version for the Fredkin chain (resp. Motzkin chain), for  $O$  in Eq. (11). The matrix element  $\mathcal{T}_{S^z}^{k_1 k_2}$  as defined by Eq. (12) is shown in appendix B to be of the form

$$\mathcal{T}_{S^z}^{k_1 k_2} = \frac{S}{L} \left( 1 - (-1)^{k_1+k_2} \right) \sin \left( \frac{\pi k_2}{L} \right) \left[ \cot \left( \frac{\pi(k_1+k_2)}{2L} \right) + \cot \left( \frac{\pi(k_1-k_2)}{2L} \right) \right], \quad (14)$$

where  $S = \frac{1}{2}$  (resp.  $S = 1$ ) for the Fredkin chain (resp. Motzkin chain). Inserting it along with the eigenvalues and vectors in Eq. (13), into Eq. (11) gives

$$\begin{aligned} \langle S_r^z \rangle &= \frac{2S}{CL^2} \sum_{k_1, k_2=1}^L \left( 1 - (-1)^{k_1+k_2} \right) \lambda_{k_1}^{r-1} \lambda_{k_2}^{2L-r} \sin \left( \frac{\pi k_1}{L} \right) \sin^2 \left( \frac{\pi k_2}{L} \right) \\ &\quad \times \left[ \cot \left( \frac{\pi(k_1+k_2)}{2L} \right) + \cot \left( \frac{\pi(k_1-k_2)}{2L} \right) \right], \end{aligned} \quad (15)$$

where we have identified  $d_{\max} + 1$  with  $L$  since we are interested in the large  $L$  limit. To make progress, we approximate the sums over  $k_1$  and  $k_2$  as integrals over  $x = \frac{\pi k_1}{L}$  and  $y = \frac{\pi k_2}{L}$ , using the standard method for replacing sums with integrals valid for large  $L$

$$\sum_{k_1, k_2=1}^L f \left( \frac{\pi k_1}{L}, \frac{\pi k_2}{L} \right) \rightarrow \frac{L^2}{\pi^2} \iint_0^\pi dx dy f(x, y). \quad (16)$$

Making the substitution Eq. (16), gives

$$\langle S_r^z \rangle = \frac{2S}{C\pi^2} \iint_0^\pi dx dy \lambda^{r-1}(x) \lambda^{2L-r}(y) \sin x \sin^2 y \left[ \cot \left( \frac{x+y}{2} \right) + \cot \left( \frac{x-y}{2} \right) \right]. \quad (17)$$

In the above equation, the fast oscillating factor  $(1 - (-1)^{k_1+k_2})$  in Eq. (15), has been set to its average value of 1. For this factor, the value changes between 0 and 2 when  $k_1 + k_2$  changes from even to odd. This corresponds to very small changes in  $x$  and  $y$ , under which the rest of the integrand changes slowly. In the regions where the cotangent factor diverges, the divergence is either canceled by the sine or cosine factors. Ultimately, the validity of the approximations made in this section will be checked against the MPS numerical results in presented at the end.

For  $q = 1$ , the normalization constant  $C$  in Eq. (17) is simply the number of Dyck walks (resp. Motzkin walks) on  $2L$  steps for the Fredkin chain (resp. Motzkin chain), see appendix D. Both numbers have closed form expression in terms of  $L$ , and for large  $L$  the numbers can be approximated using the Stirling approximation and Eq. (17) becomes

$$\langle S_r^z \rangle \approx \frac{KL^{\frac{3}{2}}}{\lambda_* \pi^{\frac{3}{2}}} \iint_0^\pi dx dy \left( \frac{\lambda(x)}{\lambda_*} \right)^{r-1} \left( \frac{\lambda(y)}{\lambda_*} \right)^{2L-r} \sin x \sin^2 y \left[ \cot \left( \frac{x+y}{2} \right) + \cot \left( \frac{x-y}{2} \right) \right], \quad (18)$$

with  $K = 1$  (resp.  $K = \frac{8\sqrt{6}}{9}$ ) for the Fredkin (resp. Motzkin chain).  $\lambda_*$  is the maximum eigenvalue as  $L \rightarrow \infty$ , which is  $\lambda_* = 2$  (resp.  $\lambda_* = 3$ ) for the Fredkin case (resp. Motzkin case).

To evaluate the double integral, we assume that  $1 \ll r \ll L$ . This means that  $r$  is on the left side, far away from the halfway point. In this regime the main contribution to the integrand comes from the region where  $x$  and  $y$  are close to either 0 or  $\pi$ . This can be understood as follows. Clearly, the main contributions to the integral come from

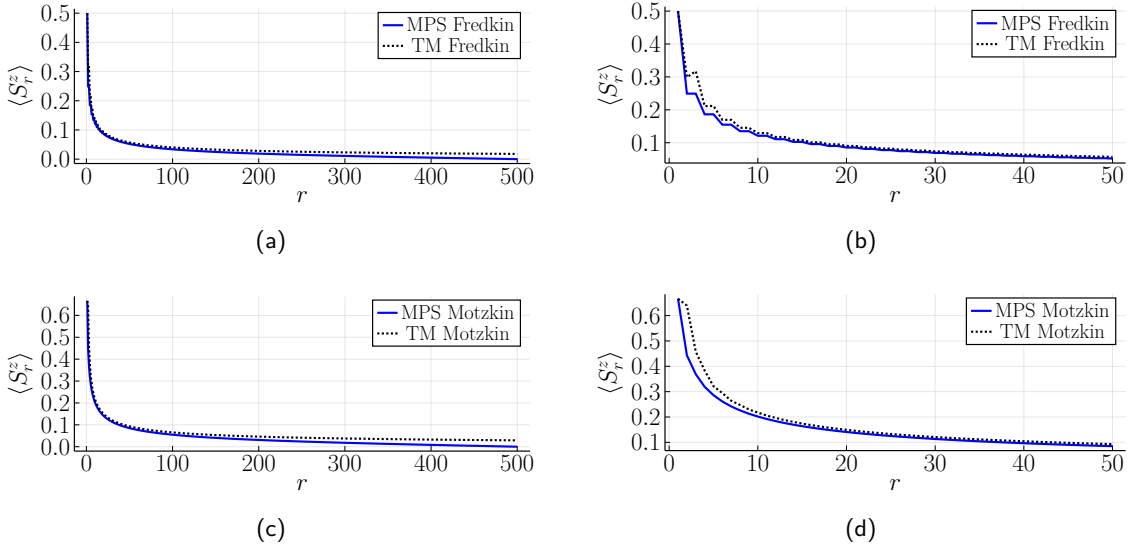


Figure 6: Comparison of  $\langle S_r^z \rangle$  obtained from the MPS ( $L = 500$ ) and from the analytic result in Eq. (19) obtained from the transfer matrix for the Fredkin and Motzkin chains. Panels (a), (b) correspond to the Fredkin chain, and panels (c), (d) to the Motzkin chain.

the vicinity of  $y = 0$  or  $y = \pi$  due to the  $\cos^{2L-r} y$ -factor, as  $(2L - r) \gg 1$ . At the same time, for small  $r$ , the  $\cos^r x$  does not constrain  $x$  to be close to 0 or  $\pi$  for the integrand in Eq. (18) to be non-vanishing. However, the  $\cot(\frac{x \pm y}{2})$  factors will diverge when  $x \rightarrow 0$  or  $x \rightarrow \pi$ , for  $y \rightarrow 0$  or  $y \rightarrow \pi$  respectively. Thus, the main contributions to the integral come from  $x = 0$  and  $x = \pi$ , also for small  $r$ . This allows for a saddle-point approximation of the double integral, which is carried out in appendix C, giving

$$\langle S_r^z \rangle \approx \begin{cases} \frac{1}{\sqrt{2\pi(r-1)}} + \frac{(-1)^{r+1}}{4\sqrt{\pi}(2(r-1))^{3/2}}, & \text{for Fredkin,} \\ \frac{4}{\sqrt{3\pi(r-1)}}, & \text{for Motzkin.} \end{cases} \quad (19)$$

This shows that  $\langle S_r^z \rangle \sim 1/\sqrt{r}$  for both the Fredkin and Motzkin chain for  $1 \ll r \ll L$ , which agrees with the combinatorial results of Ref. [32, 33] for the Motzkin chain and the field theoretic results in the scaling limit of Ref. [34] for the Fredkin chain. The corresponding critical exponent is  $\eta = \frac{3}{2}$ .

Finally, the predictions of Eq. (19) are compared with the numerical results from MPS calculations in Fig. (6). The results are in agreement for  $1 \ll r \ll L$ , when our approximations are valid. Fig. (6) (b) shows that Eq. (19) also captures the oscillations near the boundary. For the Fredkin chain odd  $r$  give larger values for  $\langle S_r^z \rangle$  than the adjacent even sites for small  $r$ . This effect vanishes as  $\sim r^{-3/2}$  as seen from Eq. (19).

## 6 RG analysis of $q$ -deformation

At  $q \neq 1$  the matrices  $T_{\max}$  in Eq. (10) are no longer Toeplitz, and their eigenvalues and eigenvectors do not have closed form expressions for arbitrary  $L$ . But the duality  $q^{2L}T(1/q) = ST(q)S^{-1}$ , (for some orthogonal matrix  $S$  that inverts the column and row indices,) implies that the ratio between the two largest magnitudes of their eigenvalues

for  $T(q)$  and  $T(1/q)$  is the same. Therefore we have  $\nu_{\pm} = \nu$ . The explicit value can be determined from the scaling dimension of  $S^z$  obtained in Eq. (19) using RG analysis.

An expression for the free energy of the ensemble of configurations in the GS has been derived for the scaling limit in Ref. [28]. The 1D lattice version can be written as

$$F_L(\sigma, \tau) = \sum_{r=1}^L \left( \sigma(S_r^z)^2 - \tau \sum_{j=1}^r S_j^z \right) = \sum_{r=1}^L \left( \sigma(S_r^z)^2 - \tau(L-r)S_r^z \right), \quad (20)$$

where  $\tau = \log q$ , and  $\sigma$  is the surface tension of the height function that correspond to the thermal parameter in the RG. Notice that the above form of the free energy is only a good approximation for  $q \neq 1$ . At the critical point, the hard wall condition at zero height becomes important for the scaling, which effectively makes all the spins in the chain strongly interacting with each other. Thus the non-interacting version of the free energy is only valid when the non-negativity of the height can be ignored compared to the spatially varying magnetic field  $\tau(L-r)$  that vanishes at  $q = 1$ .

After one step of coarse graining with block size  $b = 2$ , it becomes

$$F'_{L/b}(\sigma', \tau') = \sum_{r=1}^{L/b} \left( \sigma' (S'_r)^2 - \tau' \left( \frac{L}{b} - r \right) S'_r \right), \quad (21)$$

In order for the free energy to stay invariant, its density must satisfy  $f'(\sigma', \tau') = b f(\sigma, \tau)$ , which demands the RG equations

$$\tau' S'^z = b^2 \tau S^z, \quad \sigma' (S'^z)^2 = b \sigma (S^z)^2. \quad (22)$$

As Eq. (19) established the scaling dimension of the spin operator  $S'^z = b^{1/2} S^z$ , we must have  $\tau' = b^{3/2} \tau$  and  $\sigma' = \sigma$ . Since the correlation length changes as  $\xi'(\tau') = \xi(\tau)/b$ , we have the equation

$$\xi(b^{3/2} \tau) = \frac{\xi(\tau)}{b}, \quad (23)$$

which is solved by  $\xi(\tau) = \xi_0 \tau^{-2/3}$ , giving  $\nu = 2/3$ .

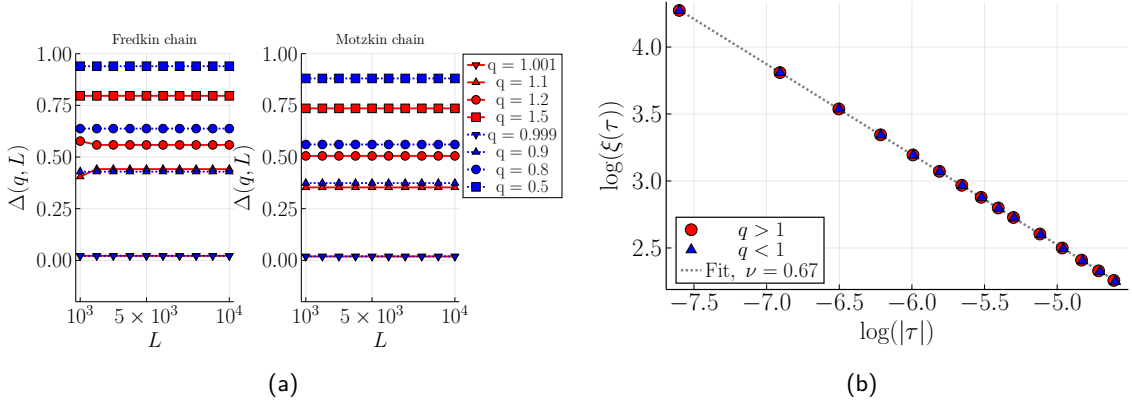


Figure 7: (a) The eigenvalue gap  $\Delta(q, L) = (\lambda_1 - \lambda_2)/\lambda_1$  as a function of the system size  $L$  for various  $qs$ . (b) Log-log plot of the correlation length  $\xi(\tau) = -1/\ln|\lambda_2/\lambda_1|$ , where  $\tau = \log q$ , for various  $q < 1$  (marked by blue circles) and  $q > 1$  (marked by red triangles), with  $L = 4000$ . The dotted gray line indicate the fit  $\xi(\tau) \sim |\tau|^{-\nu}$ . The results in (b) are for the Fredkin chain, but identical behavior is seen for the Motzkin chain.

This result is confirmed by the numerical diagonalization of the transfer matrices  $T_{\max}$ . The finite correlation length off criticality

$$\xi_{\text{TM}}(\tau) = \frac{\xi_1}{\ln \frac{\lambda_1(\tau)}{\lambda_2(\tau)}} \quad (24)$$

is given by the inverse of the logarithm of the ratio between the eigenvalues with the two largest magnitudes  $\lambda_{1,2}$ . For  $q \neq 1$ , there is a finite spectral gap of  $T_{\max}$  in the thermodynamic limit of  $d_{\max} \rightarrow \infty$ , as shown in Fig. 7 (a). The dependence of the numerical correlation length extracted from the transfer matrix  $\xi_{\text{TM}}(\tau)$  on the reduced temperature  $\tau$  as plotted in log-log scale in Fig. 7 (b) agrees with the scaling analysis from the RG.

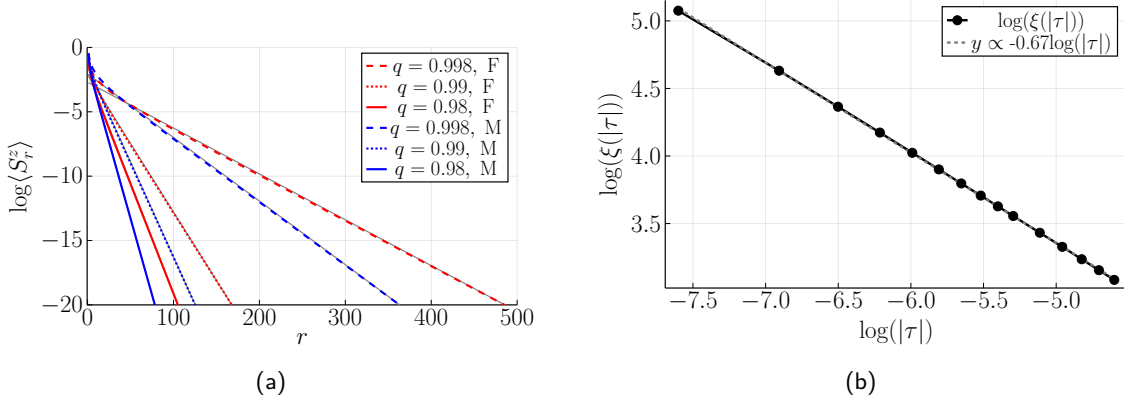


Figure 8: (a) Plot of  $\log \langle S_r^z \rangle$  in the ground state for various  $q < 1$ . The faint gray lines indicate the linear fits determining the correlation length  $\xi(q)$ . The plot is shown for the first 500 sites with  $L = 1000$  and F (resp. M) denotes Fredkin (resp. Motzkin). (b) Log-log plot of the correlation length  $\xi(|\tau|)$  for  $q < 1$ , where  $\tau = \log q$ . The dashed gray line is the line fit of slope  $\approx -0.67$ , which is almost indistinguishable from the data points marked with black dots. Note that the results shown are for the Fredkin chain, but identical results are obtained from the Motzkin chain.

Although the correlation length is finite for both the disordered ( $q < 1$ ) and ordered ( $q > 1$ ) phases, the spatial decay of the order parameter  $\langle S_r^z \rangle$  behaves quite differently in the two phases. For the disordered phase, the order parameter decays exponentially as  $\langle S_r^z \rangle = e^{-r/\xi}$  for  $1 \ll r \ll L$ , which is confirmed by the numerical results from the MPS calculation shown in Fig. 8. For the ordered phase, however, due to the opposite boundary conditions, there is a domain wall with a thickness that depends on the correlation length.

Interestingly, the dependence is different from the prediction from Ginzburg-Landau theory, where the domain wall thickness is proportional to the correlation length (see Appendix A for a derivation). In our case, the free energy Eq. (20) for the classical spin configurations in the GS superposition Eq. (20) is non-interacting. So the partition function decomposes into a product of the partition function at each individual lattice site. The expectation value of the spin  $\langle S_r^z \rangle$  can hence be calculated as

$$\langle S_r^z \rangle = S \frac{e^{\tau(L-r)} - e^{-\tau(L-r)}}{e^{\tau(L-r)} + e^{-\tau(L-r)}} = S \tanh(\tau(L-r)), \quad (25)$$

where  $S = \frac{1}{2}$  (resp.  $S = 1$ ) for the Fredkin (resp. Motzkin) chain. This novel scaling relation  $w \sim \xi^{3/2}$  between the domain wall thickness  $w \propto \tau^{-1}$  and the correlation length  $\xi \propto \tau^{-2/3}$  is also confirmed by numerical results from MPS, as shown in Fig. 9.

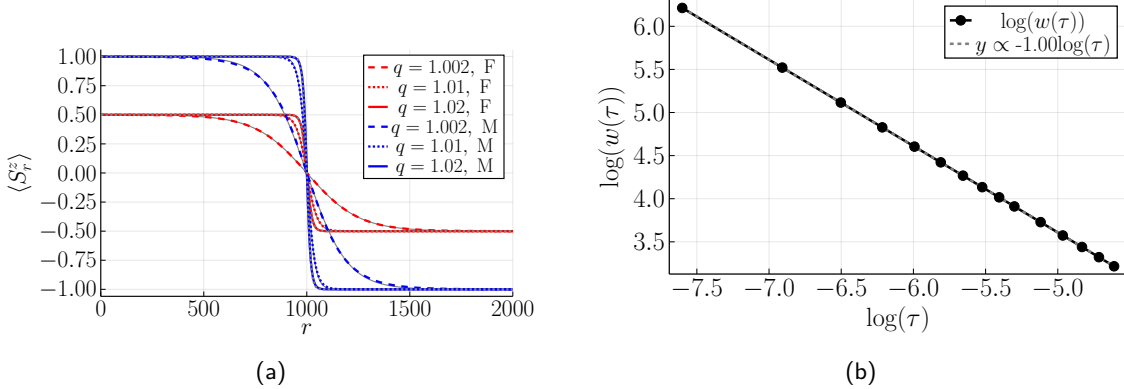


Figure 9: (a) Plot of  $\langle S_r^z \rangle$  for various  $q > 1$ , for a system of  $L = 1000$ . The faint gray lines indicate the fitted Fermi-Dirac distribution (almost indistinguishable from the data) giving the domain wall width  $w(q)$ . Note that F (resp. M) denotes Fredkin (resp. Motzkin). (b) Log-log plot of the domain wall width  $w(\tau)$ , where  $\tau = \log q$  for  $q > 1$ . The dashed gray line is the line fit of slope  $\approx -1.00$ , which is almost indistinguishable from the data points marked with black dots. Note that the results shown are for the Fredkin chain, but identical results are obtained from the Motzkin chain.

## 7 Conclusion

Much like in statistical mechanics, where the TM and the RG are the two major non-perturbative approaches for analytical solutions, the MPS (and PEPS) and the MERA are the two main methods that can render exact results on quantum many-body systems. The two types of approaches usually work for very different types of systems. The former relies on translational invariance, whereas the latter is only exact for hierarchical structures. In this paper, we saw the unification of them in the Motzkin and Fredkin GSs. This observation has lead to an exposition on the equivalence among maximal decompositions of TNs and the restoration of translational invariance in the MERA. The local swapping between an isometry and a unitary can be imposed as an extra constraint when applying the MERA as a numerical simulation for translationally invariant GSs, and potentially improve the accuracy in the description.

While TM is a well established approach for showing exponential decay of correlation functions and computing the correlation length for non-critical systems, there has not been any examples known to the authors that it is used at the critical point, where its largest eigenvalues become degenerate and the correlation length diverges. In this article, we managed to show the power-law decay of correlation and extract the critical exponent  $\eta$  using the TM obtained from the MPS representation of the Motzkin and Fredkin GSs. Furthermore, the  $q$ -deformation away from criticality can be viewed as a perturbation to the TM at the critical point, which splits the degeneracy its eigenvalues. This gives a universal value of the critical exponent  $\nu$  independent of the microscopic details of the TM.

Critical exponents are traditionally computed using RG analyses. As Vidal has pointed out [37], the coarse-grained configurations in different levels of MERA or the pentagonal TN of Fig. 1 can be considered an RG flow of GSs. Although we are able to deduce from the TM results that the effective ‘temperature’ defined by  $\tau = \log q$  has the RG eigenvalue  $y_\tau = 3/2$ , it is not clear at the moment how that could be derived from the RG transformation encoded in the TN. One future direction is therefore to perform the RG transformation according to the coarse-graining procedure given by the hierarchical TN to compute the critical exponents.

## References

- [1] Steven R. White. “Density matrix formulation for quantum renormalization groups”. *Phys. Rev. Lett.* **69**, 2863–2866 (1992).
- [2] G. Vidal. “Classical simulation of infinite-size quantum lattice systems in one spatial dimension”. *Phys. Rev. Lett.* **98**, 070201 (2007).
- [3] D. Perez-Garcia, F. Verstraete, M. M. Wolf, and J. I. Cirac. “Matrix product state representations”. *Quantum Info. Comput.* **7**, 401–430 (2007).
- [4] J. Ignacio Cirac, David Pérez-García, Norbert Schuch, and Frank Verstraete. “Matrix product states and projected entangled pair states: Concepts, symmetries, theorems”. *Rev. Mod. Phys.* **93**, 045003 (2021).
- [5] Ian Affleck, Tom Kennedy, Elliott H. Lieb, and Hal Tasaki. “Rigorous results on valence-bond ground states in antiferromagnets”. *Phys. Rev. Lett.* **59**, 799–802 (1987).
- [6] Ian Affleck, Tom Kennedy, Elliott H. Lieb, and Hal Tasaki. “Valence bond ground states in isotropic quantum antiferromagnets”. *Communications in Mathematical Physics* **115**, 477–528 (1988).
- [7] Chanchal K. Majumdar and Dipan K. Ghosh. “On next-nearest-neighbor interaction in linear chain. i”. *Journal of Mathematical Physics* **10**, 1388–1398 (1969).
- [8] Chanchal K. Majumdar and Dipan K. Ghosh. “On next-nearest-neighbor interaction in linear chain. ii”. *Journal of Mathematical Physics* **10**, 1399–1402 (1969).
- [9] Tom Kennedy, Elliott H. Lieb, and Hal Tasaki. “A two-dimensional isotropic quantum antiferromagnet with unique disordered ground state”. *Journal of Statistical Physics* **53**, 383–415 (1988).
- [10] F. Verstraete, M. M. Wolf, D. Perez-Garcia, and J. I. Cirac. “Criticality, the area law, and the computational power of projected entangled pair states”. *Phys. Rev. Lett.* **96**, 220601 (2006).
- [11] Daniel P. Arovas. “Simplex solid states of  $SU(n)$  quantum antiferromagnets”. *Phys. Rev. B* **77**, 104404 (2008).
- [12] Z. Y. Xie, J. Chen, J. F. Yu, X. Kong, B. Normand, and T. Xiang. “Tensor renormalization of quantum many-body systems using projected entangled simplex states”. *Phys. Rev. X* **4**, 011025 (2014).
- [13] G. Vidal. “Class of quantum many-body states that can be efficiently simulated”. *Phys. Rev. Lett.* **101**, 110501 (2008).
- [14] Glen Evenbly and Steven R. White. “Entanglement renormalization and wavelets”. *Phys. Rev. Lett.* **116**, 140403 (2016).
- [15] Jutho Haegeman, Brian Swingle, Michael Walter, Jordan Cotler, Glen Evenbly, and Volkher B. Scholz. “Rigorous free-fermion entanglement renormalization from wavelet theory”. *Phys. Rev. X* **8**, 011003 (2018).
- [16] J. Eisert, M. Cramer, and M. B. Plenio. “Colloquium: Area laws for the entanglement entropy”. *Reviews of Modern Physics* **82**, 277–306 (2010).
- [17] Michael Levin and Cody P. Nave. “Tensor renormalization group approach to two-dimensional classical lattice models”. *Phys. Rev. Lett.* **99**, 120601 (2007).
- [18] Zheng-Cheng Gu and Xiao-Gang Wen. “Tensor-entanglement-filtering renormalization approach and symmetry-protected topological order”. *Phys. Rev. B* **80**, 155131 (2009).

- [19] G. Evenbly and G. Vidal. “Tensor network renormalization”. *Phys. Rev. Lett.* **115**, 180405 (2015).
- [20] Sergey Bravyi, Libor Caha, Ramis Movassagh, Daniel Nagaj, and Peter W. Shor. “Criticality without frustration for quantum spin-1 chains”. *Phys. Rev. Lett.* **109**, 207202 (2012).
- [21] Rafael N. Alexander, Glen Evenbly, and Israel Klich. “Exact holographic tensor networks for the Motzkin spin chain”. *Quantum* **5**, 546 (2021).
- [22] Olof Salberger and Vladimir Korepin. “Fredkin spin chain”. *Pages 439–458*. WORLD SCIENTIFIC. (2017).
- [23] Zhao Zhang, Amr Ahmadain, and Israel Klich. “Novel quantum phase transition from bounded to extensive entanglement”. *Proceedings of the National Academy of Sciences* **114**, 5142–5146 (2017).
- [24] Olof Salberger, Takuma Udagawa, Zhao Zhang, Hosho Katsura, Israel Klich, and Vladimir Korepin. “Deformed Fredkin spin chain with extensive entanglement”. *Journal of Statistical Mechanics: Theory and Experiment* **6**, 063103 (2017).
- [25] Zhao Zhang and Israel Klich. “Entropy, gap and a multi-parameter deformation of the fredkin spin chain”. *Journal of Physics A: Mathematical and Theoretical* **50**, 425201 (2017).
- [26] Rafael N. Alexander, Amr Ahmadain, Zhao Zhang, and Israel Klich. “Exact rainbow tensor networks for the colorful motzkin and fredkin spin chains”. *Phys. Rev. B* **100**, 214430 (2019).
- [27] Zhao Zhang and Israel Klich. “Coupled Fredkin and Motzkin chains from quantum six- and nineteen-vertex models”. *SciPost Phys.* **15**, 044 (2023).
- [28] Zhao Zhang and Israel Klich. “Quantum lozenge tiling and entanglement phase transition”. *Quantum* **8**, 1497 (2024).
- [29] Zhao Zhang and Olai B. Mykland. “2d entanglement from a twisted motzkin spaghetti” (2025). [arXiv:2506.02103](https://arxiv.org/abs/2506.02103).
- [30] S.M. Lane. “Categories for the working mathematician”. *Graduate Texts in Mathematics*. Springer. (1998).
- [31] G. Evenbly and G. Vidal. “Algorithms for entanglement renormalization”. *Phys. Rev. B* **79**, 144108 (2009).
- [32] Ramis Movassagh. “Entanglement and correlation functions of the quantum motzkin spin-chain”. *Journal of Mathematical Physics* **58**, 031901 (2017).
- [33] Varun Menon, Andi Gu, and Ramis Movassagh. “Symmetries, correlation functions, and entanglement of general quantum motzkin spin-chains” (2024). [arXiv:2408.16070](https://arxiv.org/abs/2408.16070).
- [34] Olai B. Mykland and Zhao Zhang. “Highly entangled 2d ground states: Tensor networks and correlation functions” (2025). [arXiv:2502.20192](https://arxiv.org/abs/2502.20192).
- [35] Matthew Fishman, Steven White, and Edwin Stoudenmire. “The itensor software library for tensor network calculations”. *SciPost Physics Codebases* (2022).
- [36] L Dell’Anna, L Barbiero, and A Trombettoni. “Dynamics and correlations in motzkin and fredkin spin chains”. *Journal of Statistical Mechanics: Theory and Experiment* **2019**, 124025 (2019).
- [37] G. Vidal. “Entanglement renormalization”. *Phys. Rev. Lett.* **99**, 220405 (2007).

[38] Radu Andrei, Marius Lemm, and Ramis Movassagh. “The spin-one motzkin chain is gapped for any area weight  $t < 1$ ” (2022). [arXiv:2204.04517](https://arxiv.org/abs/2204.04517).

## A Domain wall thickness from mean-field theory

In this appendix, we derive the relation between domain wall thickness and correlation length from the Ginzburg-Landau (G-L) free energy

$$f(\phi(l)) = (\partial_l \phi)^2 + b\phi^2 + c\phi^4, \quad (26)$$

for the field  $\phi(l) = \langle S_l^z \rangle$ , as its spatial average is vanishing due to parity symmetry. The G-L equation

$$\partial_l^2 \phi = b\phi + 2c\phi^3 \quad (27)$$

has no explicit dependence on the variable  $l$ , so it has the first integral

$$I = f - \partial_l \phi \frac{\partial f}{\partial (\partial_l \phi)} = -(\partial_l \phi)^2 + b\phi^2 + c\phi^4, \quad (28)$$

satisfying  $\partial_l I = 0$ . Near the two boundaries, we have the two stationary solutions

$$\phi(L \mp L) = \pm \sqrt{\frac{-b}{2c}} \equiv \pm 1, \quad (29)$$

and  $\partial_l \phi|_{l=0,2L} = 0$  for  $b < 0$ . Using the conservation of the first integral, we have

$$\partial_l \phi = \sqrt{\frac{-b}{2}}(1 - \phi^2), \quad (30)$$

which integrates to

$$\phi(l) = \tanh \left( \sqrt{\frac{-b}{2}}(L - l) \right). \quad (31)$$

On the other hand, the correlation length is given by the inverse mass  $\xi = \sqrt{\frac{1}{-2b}}$  for the ordered phase  $b < 0$ . So we see the domain wall thickness predicted by the G-L theory is exactly twice the correlation length.

## B Derivation of $\mathcal{T}_{S^z}^{k_1 k_2}$ at $q = 1$

In this appendix we derive the closed form expression of  $\mathcal{T}_{S^z}^{k_1 k_2}$  in the  $q = 1$  case needed to arrive at the final expression for  $\langle S_r^z \rangle$  in Eq. (19). We start with  $\mathcal{T}_{S^z}^{k_1 k_2}$ , which is obtained by inserting the matrix representation for  $S^z$  for  $O$  in Eq. (12). Using that the eigenvectors  $|k_i\rangle$  of the maximum dimension matrix block are given by Eq. (13) gives

$$\begin{aligned} \mathcal{T}_{S^z}^{k_1 k_2} &= \langle k_1 | \mathcal{T}_{S^z} | k_2 \rangle, \\ &= \frac{2S}{d_{\max}} \sum_{j,l=1}^{d_{\max}} \sin \left( \frac{\pi k_1 j}{d_{\max} + 1} \right) (\delta_{j,l-1} - \delta_{j,l+1}) \sin \left( \frac{\pi k_2 l}{d_{\max} + 1} \right). \end{aligned} \quad (32)$$

Note that  $(\mathcal{T}_{S^z})_{jl} = S(\delta_{j,l-1} - \delta_{j,l+1})$ , with  $S = \frac{1}{2}$  for the Fredkin chain and  $S = 1$  for the Motzkin chain. This is seen by inserting the matrix representation for  $S^z$  for  $O$  in Eq. (12). Since we are interested in the large  $L$  limit, the following simplification  $d_{\max} + 1 \approx d_{\max} \approx L$  is made. Equation (32) then becomes

$$\begin{aligned}
\mathcal{T}_{S^z}^{k_1 k_2} &= \frac{4S}{L} \sin\left(\frac{\pi k_2}{L}\right) \sum_{j=1}^L \sin\left(\frac{\pi k_1 j}{L}\right) \cos\left(\frac{\pi k_2 j}{L}\right), \\
&= \frac{2S}{L} \sin\left(\frac{\pi k_2}{L}\right) \sum_{j=1}^L \left[ \sin\left(\frac{\pi(k_1 + k_2)j}{L}\right) + \sin\left(\frac{\pi(k_1 - k_2)j}{L}\right) \right],
\end{aligned} \tag{33}$$

where we have used product-to-sum trigonometric identities to obtain the final expression. The sums in Eq. (33) are performed using Lagrange's trigonometric identities, to obtain the closed form expression. Using that  $k_1$  and  $k_2$  are integers, we obtain Eq. (14). Note that for even  $k_1 + k_2$ , the expression vanishes. Inserting this expression into Eq. (11) gives Eq. (15).

## C Evaluation of integrals

In this appendix we evaluate the double integral  $I$  in Eq. (18) in the limit  $1 \ll r \ll L$ . For the Fredkin case, the main contribution of the integral comes from the region close to  $x = 0, \pi$  and  $y = 0, \pi$ . We therefore split the double integral in four terms, each capturing one of the maxima. This gives

$$I(r) = \left[ \int_0^{\frac{\pi}{2}} \int_0^{\frac{\pi}{2}} dx dy \dots + \int_0^{\frac{\pi}{2}} \int_{\frac{\pi}{2}}^{\pi} dx dy \dots + \int_{\frac{\pi}{2}}^{\pi} \int_0^{\frac{\pi}{2}} dx dy \dots + \int_{\frac{\pi}{2}}^{\pi} \int_{\frac{\pi}{2}}^{\pi} dx dy \dots \right], \tag{34}$$

where the dots refer to the integrand of Eq. (18). For each of the four terms, we perform a saddle-point approximation, by expanding the integrand around the point of maximum value. For the first term in Eq. (34),  $I_1$ , the integrand is sharply peaked around  $x = 0$  and  $y = 0$ . The saddle-point approximation is then performed by Taylor expanding the integrand in the vicinity of  $x = 0$  and  $y = 0$ , which gives

$$I_1(r) = 4 \iint_0^{\pi/2} dx dy \frac{x^2 y^2}{x^2 - y^2} e^{-\frac{(r-1)x^2}{\lambda_*}} e^{-\frac{(2L-r)y^2}{\lambda_*}}. \tag{35}$$

Here we have used that  $\cot(\frac{x \pm y}{2}) \approx \frac{2}{x \pm y}$  for  $x$  and  $y$  close to 0 and Taylor expanded the cos-functions followed by an exponential approximation. To proceed, notice that the exponential functions quickly vanish as  $x$  and  $y$  increase. The characteristic width of the exponential functions are  $\sim \lambda_*/\sqrt{r-1}$  and  $\sim \lambda_*/\sqrt{2L-r}$ , both fully contained within the integration limits when  $1 \ll r \ll L$ . We therefore extend the limit to infinity without affecting the result significantly

$$I_1(r) \approx 4 \iint_0^{\infty} dx dy \frac{x^2 y^2}{x^2 - y^2} e^{-\frac{(r-1)x^2}{\lambda_*}} e^{-\frac{(2L-r)y^2}{\lambda_*}}. \tag{36}$$

Next, we perform substitutions  $u = x\sqrt{\frac{2(r-1)}{\lambda_*}}$  and  $v = y\sqrt{\frac{2(2L-r)}{\lambda_*}}$ , giving

$$\begin{aligned}
I_1(r) &= \frac{4\lambda_*^2}{2^2 \sqrt{(r-1)(2L-r)}} \iint_0^{\infty} du dv \frac{u^2 v^2}{(2L-r)u^2 - (r-1)v^2} e^{-\frac{u^2}{2}} e^{-\frac{v^2}{2}}, \\
&= \frac{\lambda_*^2}{(2L)^{3/2} \sqrt{(r-1)(1 - \frac{r}{2L})}} \iint_0^{\infty} du dv \frac{u^2 v^2}{(1 - \frac{r}{2L})u^2 - \frac{r-1}{2L}v^2} e^{-\frac{u^2}{2}} e^{-\frac{v^2}{2}}.
\end{aligned} \tag{37}$$

In the limit  $r \ll L$ , it becomes an elementary integral

$$I_1(r) \approx \frac{\lambda_*^2}{(2L)^{3/2}\sqrt{r-1}} \iint_0^\infty du dv v^2 e^{-\frac{u^2}{2}} e^{-\frac{v^2}{2}} = \frac{\pi \lambda_*^2}{2(2L)^{3/2}\sqrt{r-1}}. \quad (38)$$

Next up is the second term in Eq. (34),  $I_2$ , where we perform the expansions around  $x = 0$  and  $y = \pi$ . For the Motzkin chain, this produces a term that vanishes as  $3^{r-2L}$ . For the Fredkin chain this gives

$$\begin{aligned} I_2(r) &= (-1)^{2L-r} \int_0^{\pi/2} \int_{\pi/2}^\pi dx dy (-x^2)(\pi-y)^2 e^{-\frac{(r-1)x^2}{2}} e^{-\frac{(2L-r)(\pi-y)^2}{2}}, \\ &= (-1)^{r+1} \int_0^{\pi/2} \int_0^{\pi/2} dx dy x^2 y^2 e^{-\frac{(r-1)x^2}{2}} e^{-\frac{(2L-r)y^2}{2}}, \end{aligned} \quad (39)$$

following the same steps as for  $I_1$ . Note that the  $(-1)^p$  term results from expanding  $\cos^p(y)$  around  $y = \pi$ . To obtain the second line in Eq. (39), we have performed the substitution  $y' = \pi - y$  and switched upper and lower limits. Following the same steps as for  $I_1$ , Eq. (39) is evaluated as

$$\begin{aligned} I_2(r) &\approx (-1)^{r+1} \iint_0^\infty dx dy x^2 y^2 e^{-\frac{(r-1)x^2}{2}} e^{-\frac{(2L-r)y^2}{2}}, \\ &= \frac{(-1)^{r+1}}{(2L)^{3/2}(r-1)^{3/2}} \iint_0^\infty du dv u^2 v^2 e^{-\frac{u^2}{2}} e^{-\frac{v^2}{2}}, \\ &= \frac{(-1)^{r+1}\pi}{2(2L)^{3/2}(r-1)^{3/2}}. \end{aligned} \quad (40)$$

For the Fredkin chain, the last two terms in Eq. (34),  $I_3$  and  $I_4$ , are found to be identical to  $I_2$  and  $I_1$  respectively. For  $I_3$  this is seen by expanding around  $x = \pi$  and  $y = 0$  and then substituting  $x' = \pi - x$ . For  $I_4$  this is seen by expanding around  $x = \pi$  and  $y = \pi$  and performing the same substitution for both  $x$  and  $y$ . Thus, we have found

$$I_{\text{Fredkin}}(r) \approx 2 [I_1(r) + I_2(r)]. \quad (41)$$

For the Motzkin case, because the spectrum of the transfer matrix is asymmetric about 0, its largest eigenvalues are located in the region where both  $x$  and  $y$  are near 0. So there is no need to split the integral, and it is safe to extend the upper boundary of the integrals  $\pi$  to infinity. So the result is identical with Eq. (38) for the Fredkin case, differing only in the value of  $\lambda_*$ .

## D Fredkin and Motzkin spin chains

In this appendix we briefly present the GSs of the deformed Fredkin and Motzkin chains, and their respective parent Hamiltonians. The GSs of the models can be described in terms of two types of walks on the  $(x, y)$  grid. The Fredkin GS is described by Dyck walks, while the Motzkin GS by Motzkin walks. A Dyck walk of  $2L$  steps is defined as a path on the  $(x, y)$  grid, consisting of up steps  $(1, 1)$  and down steps  $(1, -1)$  starting from  $(0, 0)$  and ending at  $(2L, 0)$ , that never passes below the  $x$ -axis. The Motzkin walk is described by the same definition, but in addition they are diluted by flat steps, that is, also the step  $(1, 0)$  is valid. Examples of Dyck walks are seen in Fig. (10) (a) and (b) whereas all walks in Fig. (10) are examples of Motzkin walks.

Each walk is associated to a specific state in the Hilbert space  $\mathcal{H}^{\otimes 2L}$  of the spin chain, where  $\mathcal{H}$  is the Hilbert space of each spin and  $\otimes$  denotes the tensor product. For the spin- $\frac{1}{2}$

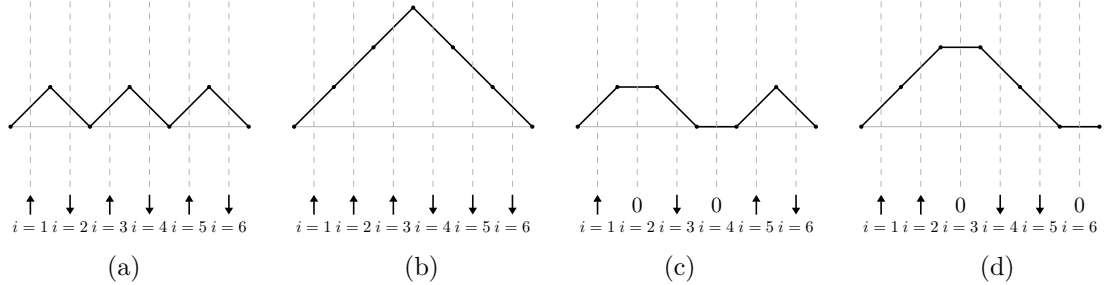


Figure 10: Spin configurations and corresponding Motzkin walks for  $L = 3$ . (a) and (b) are also Dyck walks, while (c) and (d) are not.

Fredkin chain (resp. spin-1 Motzkin chain)  $\mathcal{H}$  is 2- (resp. 3-)dimensional. Specifically, the walks are associated to eigenstates of the spin operator in the  $z$  direction relating to a given spin  $i$ , denoted  $\hat{S}_i^z$ . It acts non-trivially only on the  $i$ th spin, that is

$$\hat{S}_i^z = \hat{1}^{\otimes(i-1)} \otimes \hat{S}^z \otimes \hat{1}^{\otimes(2L-i)}, \quad (42)$$

where  $\hat{1}$  is the identity operator. We denote the eigenstates of the operator  $\hat{S}^z$  as  $|\uparrow\rangle$  and  $|\downarrow\rangle$ , which has eigenvalues  $\pm\frac{1}{2}$  in the Fredkin case and  $\pm 1$  in the Motzkin case. Additionally, we have the eigenstate  $|0\rangle$  of eigenvalue 0 in the Motzkin case. We let walks represent states of the chain by making the correspondence between a spin at position  $i$  in the chain and a step taken at position  $i - 1/2$  in the walk in the following way

$$|\uparrow\rangle_i \leftrightarrow (1, 1)_{i-1/2}, \quad |\downarrow\rangle_i \leftrightarrow (1, -1)_{i-1/2}, \quad |0\rangle_i \leftrightarrow (1, 0)_{i-1/2}. \quad (43)$$

This correspondence is seen in Fig. (10), where the subscript  $i - 1/2$  indicate the midpoint between spins, marked by black dots. Clearly, states described by walks using the correspondence Eq. (43) is a mutual eigenstate of all operators  $\hat{S}_i^z$ , meaning that

$$\hat{S}_i^z |w\rangle = c |w\rangle, \quad \forall i, \quad (44)$$

where  $c = \pm\frac{1}{2}$  for the Fredkin chains and  $c = 0, \pm 1$  for the Motzkin chain. We call such states  $|w\rangle$  spin configurations.

Using the correspondence Eq. (43), the unique GSs of the deformed Fredkin and Motzkin chain  $|\text{GS}(q)\rangle$ , can be expressed as

$$|\text{GS}(q)\rangle = \frac{1}{\sqrt{C}} \sum_{w \in D_{2L}} q^{A(w)} |w\rangle, \quad (45)$$

where  $C$  is a normalization constant and  $D_{2L}$  is the set of all Dyck or Motzkin walks on  $2L$  steps, depending on which model we consider. Note also that  $A(w)$  is the total area beneath the walk  $w$  and that  $q$  is the deformation parameter. Clearly, at  $q = 1$  all walks are weighted equally, but at  $q > 1$  (resp.  $q < 1$ ) high area walks (resp. low area walks) are weighted more.

To understand the unusual entanglement properties of the state in Eq. (45), one can perform a Schmidt decomposition at the midpoint of the spin chain. Following [24], this gives

$$\begin{aligned}
|\text{GS}(q)\rangle &= \sum_{m=1}^{d^L} \alpha_m |\psi_m^{1,\dots,L}\rangle \otimes |\psi_m^{L+1,\dots,2L}\rangle, \\
&= \sum_{m=0}^L \sqrt{p_{L,m}(q)} |C_{0,m}^{1,\dots,L}\rangle \otimes |C_{m,0}^{L+1,\dots,2L}\rangle,
\end{aligned} \tag{46}$$

where  $d$  is the dimension of the Hilbert space  $\mathcal{H}$  of each spin, with  $d = 2$  (resp.  $d = 3$ ) for the Fredkin (resp. Motzkin) chain. Note that the states  $|C_{a,b}^{i,\dots,j}\rangle$  are area weighted superpositions of spin configurations with either  $a$  excess down spins or  $b$  excess up spins on the spins  $i$  to  $j$ . In [20, 22, 23, 24], analysis of the Schmidt coefficients  $\sqrt{p_{L,m}(q)}$  were made, which revealed that the GSs undergo a quantum criticality at the  $q = 1$  point. The GSs satisfy the area law of EE both for the ordered phase  $q > 1$  and the disordered  $q < 1$  phase, but have logarithmically scaling entanglement entropy at the critical point  $q = 1$ . Our transfer matrix approach in Sec. 4 and 5 combined with the RG analysis in Sec. 6 showed that both the ordered and disordered phases have exponentially decaying correlations. On the other hand, the gapless critical point exhibits power-law decay of correlations. These results are summarized in the phase diagram in Fig. (11). Note that the exponential decay of correlations in the ordered phase does not imply a spectral gap of the Hamiltonian. In fact, Ref. [25] has established an exponentially small upper bound on the spectral gap. This is due to the boundary magnetic field in the Hamiltonian lifting the otherwise exponentially degenerate GSs with different magnetizations to a unique GS with  $S_{\text{tot}}^z = 0$ . This boundary effect turns out not to be important for the disordered phase, so the  $q < 1$  phase is indeed gapped [38].

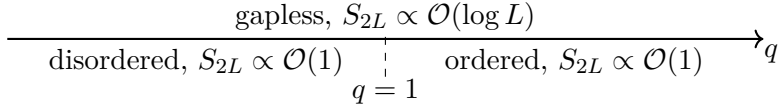


Figure 11: Phase diagram of the deformed Fredkin and Motzkin spin chain, showing how the entanglement entropy  $S_{2L}$  for the half chain partition of spin chain of length  $2L$ , undergoes a phase transition at the critical point  $q = 1$ . The entanglement entropy is bounded for both  $q > 1$  and  $q < 1$ , but shows a logarithmic violation of the area law at  $q = 1$ .

The parent Hamiltonians of the GSs can both be written as a sum of projectors onto states written in terms of the eigenstates of the single site  $\hat{S}^z$  operator. The Hamiltonian is written as

$$H_{\text{tot}}^{\text{F/M}}(q) = |\downarrow\rangle_1\langle\downarrow| + |\uparrow\rangle_{2L}\langle\uparrow| + \sum_{i=2} \Pi_i^{\text{F/M}}(q), \tag{47}$$

where  $q$  is the deformation parameter and the sum over  $\Pi_i^{\text{F/M}}(q)$  terminates at  $i = 2L - 1$  (resp.  $i = 2L$ ) for the Fredkin (resp. Motzkin) Hamiltonian. The projectors  $\Pi_i^{\text{F/M}}(q)$  are defined as

$$\Pi_i^{\text{F}}(q) = |F_i^1\rangle\langle F_i^1| + |F_i^2\rangle\langle F_i^2|, \quad \Pi_i^{\text{M}}(q) = |M_i^1\rangle\langle M_i^1| + |M_i^2\rangle\langle M_i^2| + |M_i^3\rangle\langle M_i^3|. \tag{48}$$

The  $q$ -dependent state vectors in the Fredkin projector  $\Pi_i^{\text{F}}(q)$  are defined as

$$\begin{aligned}
|F_i^1\rangle &= \frac{1}{\sqrt{q^{-2} + q^2}} (q^{-1} |\uparrow_{i-1} \uparrow_i \downarrow_{i+1}\rangle - q |\uparrow_{i-1} \downarrow_i \uparrow_{i+1}\rangle), \\
|F_i^2\rangle &= \frac{1}{\sqrt{q^{-2} + q^2}} (q^{-1} |\uparrow_{i-1} \downarrow_i \downarrow_{i+1}\rangle - q |\downarrow_{i-1} \uparrow_i \downarrow_{i+1}\rangle),
\end{aligned} \tag{49}$$

whereas the  $q$ -dependent state vectors in the Motzkin projector are defined as

$$\begin{aligned}
|M_i^1\rangle &= \frac{1}{\sqrt{1+q^2}} (|\uparrow_{i-1} 0_i\rangle - q |0_{i-1} \uparrow_i\rangle), \\
|M_i^2\rangle &= \frac{1}{\sqrt{1+q^2}} (|0_{i-1} \downarrow_i\rangle - q |\downarrow_{i-1} 0_i\rangle), \\
|M_i^3\rangle &= \frac{1}{\sqrt{1+q^2}} (|\uparrow_{i-1} \downarrow_i\rangle - q |0_{i-1} 0_i\rangle).
\end{aligned} \tag{50}$$

The states in the superpositions in  $|F_i^j\rangle$  and  $|M_i^j\rangle$  are related by the so-called Fredkin moves  $F_i^j$  and Motzkin moves  $M_i^j$ , seen in Fig. (12). Note that the Fredkin projectors involve three spins, so the model includes next-nearest-neighbor interactions. Motzkin projectors involve only two spins, so the interactions are limited to nearest neighbors. Also note the  $q$ -factors in Eq. (49) and Eq. (50) are different. This can be understood in terms of the walks associated to the spin configurations, as seen in Fig. (12). Clearly, the area under the walk segments differs by 2 units for the Fredkin case but only 1 unit for the Motzkin case. In order to ensure that the weighting of the spin configurations in Eq. (45) gives the correct GS, the low-area spin configurations are weighted with a factor  $q^2$  (resp.  $q$ ) more than the high-area spin configuration in the Fredkin case (resp. Motzkin case), in Eq. (49) and Eq. (50). The Hamiltonians  $H_{\text{tot}}^{\text{F/M}}$  are frustration free, meaning that the GSs are the lowest energy eigenstate of each individual term in Eq. (47), with GS energy 0. That is, the GSs are annihilated by each individual projector.

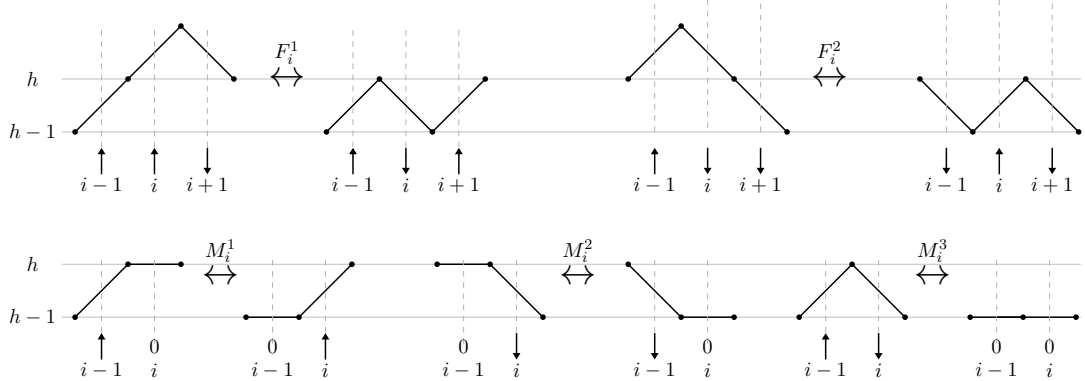


Figure 12: Upper panel: the two Fredkin moves  $F_i^1$  and  $F_i^2$  related to the states in Eq. (49). Moving from left to right reduces the area under the walk segment by 2 units. Lower panel: the three Motzkin moves  $M_i^1$ ,  $M_i^2$  and  $M_i^3$  related to the states in Eq. (50). Moving from left to right reduces the area under the walk segment by 1 unit. The solid gray lines indicate the height.

The fact that  $H_{\text{tot}}^{\text{F/M}}$  give the GS in Eq. (45) can be understood in terms of the Fredkin and Motzkin moves. First note that the boundary terms in Eq. (47) penalizes any spin configuration with a down spin at  $i = 1$  and/or an up spin at  $i = 2L$ , with an energy contribution. Thus, in order for a state to be annihilated by the boundary projectors

in Eq. (47), none of the spin configuration present in the state can start with a down spin and/or end with an up spin. Next, to construct a state that is annihilated by all bulk terms  $\Pi_i^{F/M}(q)$ , one can start from a given spin configuration and then include spin configurations related by a Fredkin or Motzkin move at  $i$  in the state. By doing this for all  $i$  and for all included spin configurations, we can assure that each  $\Pi_i^{F/M}(q)$  is annihilated by weighting the spin configurations correctly. As previously mentioned, the correct weighting is determined by looking at Fig. (12), where Fredkin (resp. Motzkin) moves relate spin configurations that differ in 2 area units (resp. 1 area unit) under the line segments traced out by the walk. In Eq. (49) and Eq. (50), we have weighted the low-area configurations with a factor  $q^2$  (resp.  $q$ ) more than the high-area configuration in the Fredkin case (resp. Motzkin case). That is, the low-area configuration is weighted a factor  $q^{\Delta A}$  more, where  $\Delta A$  is the difference in area under the walks. This implies that the correct weighting of the configurations in the GS for the projector  $\Pi_i^{F/M}(q)$  to be annihilated is to weight the high-area configuration a factor of  $q^{\Delta A}$  more than the low area configuration. This is achieved by weighting each Dyck walk  $w$  by a factor  $q^{A(w)}$ , where  $A(w)$  is the area beneath the walk  $w$ . This is exactly what is done in the GS in Eq. (45).

Finally, note that by applying a Fredkin move  $F_j^i$  (resp. Motzkin move  $M_i^j$ ) to a spin configuration described by a Dyck walk (resp. Motzkin walk), one always gets another Dyck walk (resp. Motzkin walk). Starting from a spin configuration and including all spin configurations related by a series of Fredkin moves, will always lead to a state annihilated by all  $\Pi_i^{F/M}(q)$ , but only if the initial spin configuration is described by a Dyck walk (resp. Motzkin walk) will this procedure lead to a state that is annihilated by the boundary terms in Eq. (47). For example, if we start from a spin configuration described by a walk that reaches negative height at some point, successive Fredkin or Motzkin moves will show that we are forced to include a spin configuration where the spin at  $i = 1$  is a down spin in order to make sure that the projector  $\Pi_2^{F/M}(q)$  is annihilated. Similarly, if we start from a state described by a walk that ends at a positive height, successive Fredkin moves (resp. Motzkin moves) shows that we are forced to include a state with an up spin at  $i = 2L$  in order to make sure  $\Pi_{2L-1}^F(q)$  (resp.  $\Pi_{2L}^M(q)$ ) is annihilated. In total, this means that the GSs of the models are given by the are weighted superposition of Dyck or Motzkin walks in Eq. (45).